



PERGAMON

International Journal of Plasticity 19 (2003) 365–382

INTERNATIONAL JOURNAL OF  
**Plasticity**

www.elsevier.com/locate/ijplas

## A study of microbend test by strain gradient plasticity

W. Wang<sup>a</sup>, Y. Huang<sup>b,\*</sup>, K.J. Hsia<sup>c</sup>, K.X. Hu<sup>d</sup>, A. Chandra<sup>e</sup>

<sup>a</sup>*GTSS, Motorola, 1301 Algonquin Rd., Rm 1043, Schaumburg, IL 60196, USA*

<sup>b</sup>*Department of Mechanical and Industrial Engineering, University of Illinois at Urbana-Champaign, Urbana, IL 61801, USA*

<sup>c</sup>*Department of Theoretical and Applied Mechanics, University of Illinois at Urbana-Champaign, Urbana, IL 61801, USA*

<sup>d</sup>*GlobeSpan Inc., 100 Schulz Drive, Red Bank, NJ 07701, USA*

<sup>e</sup>*Department of Mechanical Engineering, Iowa State University, Ames, IA 50011, USA*

Received in final revised form 30 August 2001

---

### Abstract

Metallic materials display strong size effect when the characteristic length associated with plastic deformation is on the order of microns. This size effect cannot be explained by classical plasticity theories since their constitutive relations do not have an intrinsic material length. Strain gradient plasticity has been developed to extend continuum plasticity to the micron or submicron regime. One major issue in strain gradient plasticity is the determination of the intrinsic material length that scales with strain gradients, and several microbend test specimens have been designed for this purpose. We have studied different microbend test specimens using the theory of strain gradient plasticity. The pure bending specimen, cantilever beam, and the microbend test specimen developed by Stolken and Evans (Stolken, J.S., Evans, A.G., 1998. A microbend test method for measuring the plasticity length scale *Acta Mater.* 46, 5109–5115) are found suitable for the determination of intrinsic material length in strain gradient plasticity. However, the double cantilever beam (both ends clamped) is unsuitable since its deformation is dominated by axial stretching. The strain gradient effects significantly increase the bending stiffness of a microbend test specimen. The deflection of a 10- $\mu\text{m}$  thick beam is only a few percent of that estimated by classical plasticity. © 2002 Elsevier Science Ltd. All rights reserved.

*Keywords:* Strain gradient plasticity; Microbend test

---

\* Corresponding author. Tel.: +1-217-265-5072; fax: +1-217-244-6534.

E-mail address: huang9@uiuc.edu (Y. Huang).

## 1. Introduction

Ultra-thin beams have been widely used in micro-electro-mechanical systems (MEMS), sensors and actuators (Chau et al., 1991; Geijselers and Tjeldeman, 1991). The thickness of these beams ranges typically from submicrons to ten microns. Within this range, metallic materials display strong size effects. For example, in the microtorsion test of thin copper wires, Fleck et al. (1994) observed that the normalized shear strength increases by a factor of 3 as the wire diameter decreases from 170 to 12  $\mu\text{m}$ . In the microbend test of thin nickel beams, Stolken and Evans (1998) observed a significant increase in plastic work hardening as the beam thickness decreases from 50 to 12.5  $\mu\text{m}$ . In the micro-indentation tests, the measured indentation hardness of metals increases by a factor of two to three as the width of the indenter decreases from 10 to 1  $\mu\text{m}$  (Nix, 1988; Stelmashenko et al., 1993; Ma and Clarke, 1996; Poole et al., 1996; McElhaney et al., 1998). For an aluminum-magnesium matrix reinforced by silicon carbide particles, Lloyd (1994) observed a substantial increase in strength as the particle diameter was reduced from 16 to 7.5  $\mu\text{m}$  at a fixed particle volume fraction of 15%. Rhee et al. (1994a,b), Zhu and Zbib (1995), Nan and Clarke (1996), and Zhu et al. (1997) also made a similar observations of size effect in metal-matrix composites. These phenomena are all related to the plastic deformation of materials at the micron scale, but cannot be explained by the classical plasticity theories because their constitutive models do not have an internal material length scale.

In order to extend continuum plasticity to the micron or submicron scale, strain gradient plasticity theories have been developed (Dillon and Kratochvil, 1970; Aifantis, 1987; Fleck and Hutchinson, 1993, 1997; Fleck et al., 1994; Gao et al., 1999; Acharya and Bassani, 2000; Huang et al., 2000a,b; Shu and Barlow, 2000; Dai and Parks, 2001; Gurtin, in press; Hwang et al., in press; Engelen et al., in press). The recent strain gradient theories are based on dislocation mechanics, which suggests that the plastic work hardening of materials is due to both statistically stored dislocations and geometrically necessary dislocations (Nye, 1953; Cottrell, 1964; Ashby, 1970), and the latter are directly related to the gradients of plastic strain. Fleck and Hutchinson (1993, 1997) and Fleck et al. (1994) have developed a phenomenological theory of strain gradient plasticity by generalizing classical  $J_2$  plasticity within the framework of higher-order continuum theory (Toupin, 1962; Koiter, 1964; Mindlin, 1964, 1965). While stresses are work conjugates for strains, couple stresses are introduced as the work conjugates for strain gradients. A length parameter,  $l$ , scales the strain gradients in the constitutive model so as to balance the dimensions of strains and strain gradients, i.e.  $\varepsilon$  and  $l(d\varepsilon/dx)$ . The length  $l$  is assumed to be an intrinsic *material length*. Based on Fleck et al. (1994) microtorsion test of thin copper wires and Stolken and Evans' (1998) microbend test of thin nickel beams, the material length  $l$  is estimated to be 4  $\mu\text{m}$  for copper and 5  $\mu\text{m}$  for nickel. As the representative length  $L$  of the deformation field becomes significantly larger than the material length  $l$ , i.e.  $L \gg l$ , strain gradient effects become negligible because the strain gradient terms are much smaller than the strains, i.e.  $l(d\varepsilon/dx) \ll \varepsilon$ , and the strain gradient plasticity theory (Fleck and Hutchinson, 1993, 1997; Fleck et al.,

1994) degenerates to classical  $J_2$  plasticity. However, as in aforementioned experiments, when the representative length  $L$  of the deformation field becomes comparable to the material length  $l$  ( $\sim \mu\text{m}$ ), strain gradient effects become significant because the strain gradient term is on the same order as the strain.

A major issue in strain gradient plasticity is the determination of the constitutive length parameter  $l$ . Are there experiments to validate that  $l$  is indeed a material length (i.e. independent of loadings and specimens)? How is it related to microstructure in a material? Based on the Taylor model in dislocation mechanics, Nix and Gao (1998) have identified this length  $l$  as  $L_d^2/b$ , where  $L_d$  is the average spacing between dislocations at plastic yield, and  $b$  is the Burgers vector. This intrinsic material length  $l$  can also be expressed as  $3\alpha^2(\frac{G}{\sigma_Y})^2 b$ , where  $\alpha$  is a constant coefficient in the Taylor model and is on the order of 1 (Nix and Gibling, 1985),  $G$  is the shear modulus, and  $\sigma_Y$  is the yield stress in uniaxial tension. As shown in Fig. 1, the micro-indentation hardness predicted by Nix and Gao's strain gradient model agreed remarkably well with the experimental data. This motivated Gao et al. (1999) and Huang et al. (2000a,b) to develop a mechanism-based strain gradient (MSG) plasticity theory based on the Taylor model in dislocation mechanics.

There are some experimental efforts to determine the material length  $l$  by microbend test of thin foils. Stolken and Evans (1998) developed a versatile microbend test, which involved the bending of a thin annealed nickel foil around a small diameter cylindrical tungsten mandril, followed by measurement of the unloaded and loaded radii of curvature. By using mandrils which have different diameters (from 125  $\mu\text{m}$  to 2 mm) as well as foils with different thickness (from 12.5 to 50  $\mu\text{m}$ ), the length scale associated with

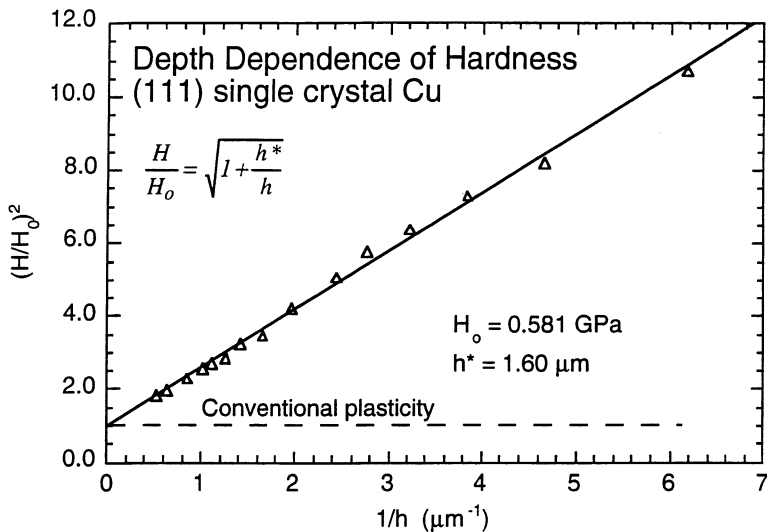


Fig. 1. Depth dependence of the hardness of (111) single crystal copper (Nix and Gao, 1998), where  $H$  is the microindentation hardness,  $H_0$  is the hardness for large depth of indentation,  $h$  is the depth of indentation; the triangles are experimental data, while the solid and dashed lines are predictions by strain gradient plasticity and conventional plasticity, respectively.

strain gradient plasticity was determined to be approximately 6  $\mu\text{m}$  for nickel. Haque and Saif (in press) used the micro-electro-mechanical systems (MEMS) to measure the force and deflection of a submicron-thick aluminum cantilever beam. The method was an extension of that developed by Saif and MacDonald (1998) for silicon-based microinstruments for atomic scale surface imaging and modifications, as well as for submicron scale material investigations. The deflection was measured to an accuracy of a few nanometers.

The beams in these microbend experiments undergo large rotations. The initially horizontal beam was bent to a nearly vertical configuration in Stolken and Evans' experiment (1998). Aifantis (1999) investigated bending of a thin beam under infinitesimal deformation. This paper provides a study of different microbend test specimens (Stolken and Evans, 1998; Haque and Saif, in press) by the phenomenological theory of strain gradient plasticity (Fleck and Hutchinson, 1993; Fleck et al., 1994). The effect of finite rotation of the beam is accounted for in the analysis. A summary of the phenomenological theory of strain gradient plasticity is given in Section 2. The pure bending specimen, the cantilever beam, and Stolken and Evans' (1998) microbend test specimen are studied in Sections 3, 4 and 5, respectively. The intrinsic material length  $l$  in strain gradient plasticity can be determined from these microbend tests in conjunction with the present analysis. It can then be used to verify the estimate based on the Taylor model in dislocation mechanics given by Nix and Gao (1998).

## 2. Strain gradient plasticity

The equilibrium equations and constitutive law in phenomenological strain gradient plasticity (Fleck and Hutchinson, 1993; Fleck et al., 1994) are summarized in this section for plane-strain deformation. The in-plane Cauchy stresses  $t_{\alpha\beta}$  ( $\alpha, \beta = 1, 2$ ) are decomposed into the symmetric part  $\sigma_{\alpha\beta}$  ( $\sigma_{\alpha\beta} = \sigma_{\beta\alpha}$ ) and the anti-symmetric part  $\tau_{\alpha\beta}$  ( $\tau_{\alpha\beta} = -\tau_{\beta\alpha}$ ). The non-vanishing couple stresses (moments per unit area) are denoted by  $m_\alpha$  ( $\alpha = 1, 2$ ), where  $m_\alpha$  stands for  $m_{\alpha 3}$  in three-dimensional strain gradient plasticity, and  $x_3$  is the out-of-plane direction. Equilibrium of forces and moments requires

$$t_{\beta\alpha, \beta} = \sigma_{\beta\alpha, \beta} + \tau_{\beta\alpha, \beta} = 0 \quad \alpha = 1, 2, \quad (1)$$

and

$$m_{\beta, \beta} + \tau_{12} - \tau_{21} = 0. \quad (2)$$

The stress traction  $\mathbf{T}$  and couple-stress traction  $\mathbf{q}$  on the boundary are

$$T_\alpha = \eta_\beta t_{\beta\alpha}, \quad q_\alpha = \eta_\beta m_{\beta\alpha}, \quad \alpha = 1, 2, \quad (3)$$

where  $\mathbf{n}$  is the unit normal vector on the boundary.

The relations among strains  $\varepsilon_{\alpha\beta}$ , displacements  $u_\alpha$ , rotation  $\omega$ , and curvatures  $\chi_\alpha$  are

$$\varepsilon_{\alpha\beta} = (u_{\alpha,\beta} + u_{\beta,\alpha})/2, \quad \omega = (u_{2,1} - u_{1,2})/2, \quad \chi_\alpha = \omega_{,\alpha}, \quad \alpha, \beta = 1, 2, \quad (4)$$

where  $\chi_\alpha$  stands for  $\chi_{3\alpha}$  in three-dimensional strain gradient plasticity. The elimination of displacements and rotations yields the  $\chi$ - $\varepsilon$  compatibility equations,

$$\chi_1 = \varepsilon_{12,1} - \varepsilon_{11,2}, \quad \chi_2 = \varepsilon_{22,1} - \varepsilon_{21,2}, \quad (5)$$

and the  $\chi$  compatibility equation,

$$\chi_{1,2} - \chi_{2,1} = 0. \quad (6)$$

In the deformation theory of phenomenological strain gradient plasticity, stresses and couple stresses are work conjugates of strains and curvatures, i.e.

$$\sigma_{\alpha\beta} = \frac{\partial W}{\partial \varepsilon_{\beta\alpha}}, \quad m_\alpha = \frac{\partial W}{\partial \chi_\alpha}, \quad \alpha, \beta = 1, 2, \quad (7)$$

where  $W$  is the strain energy density, which depends not only on the first invariant  $\varepsilon_m$  and second invariant  $\varepsilon_e$  of strains (as in classical plasticity), but also on the second invariant  $\chi_e$  of curvatures (the first invariant  $\chi_{kk}$  is zero), i.e.

$$W = W(\varepsilon_e, l\chi_e, \varepsilon_m). \quad (8)$$

Here, the intrinsic material length  $l$  enters from dimensional considerations. For plane-strain deformation, these invariants are given by

$$\varepsilon_e = \sqrt{\frac{2}{3} \left( \varepsilon_{\alpha\beta} \varepsilon_{\alpha\beta} - \frac{1}{3} \varepsilon_{\alpha\alpha} \varepsilon_{\beta\beta} \right)}, \quad \chi_e = \sqrt{\frac{2}{3} \chi_\alpha \chi_\alpha}, \quad \varepsilon_m = \varepsilon_{\alpha\alpha}. \quad (9)$$

The microtorsion test (Fleck et al., 1994) and microbend tests (Stolken and Evans, 1998; Haque and Saif, in press) are dominated by plastic deformation since the strain exceeded 10% or even 50% such that the elastic deformation is negligible. For a power-law hardening material, the strain energy density  $W$  in strain gradient plasticity takes the form

$$W = \frac{n}{n+1} \sigma_0 \varepsilon_0 \left( \frac{\bar{\varepsilon}}{\varepsilon_0} \right)^{\frac{n+1}{n}}, \quad (10)$$

where  $n$  is the plastic work hardening exponent,  $\sigma_0$  is identified as a measure of the tensile yield stress,  $\varepsilon_0 = \sigma_0/E$ ,  $E$  is the Young's modulus, and  $\bar{\varepsilon}$  is the combined measure of effective strain  $\varepsilon_e$  and effective curvature  $\chi_e$ , given by

$$\bar{\varepsilon} = (\varepsilon_e^2 + l^2 \chi_e^2)^{1/2}. \quad (11)$$

When curvatures become negligible, i.e.  $l\chi_e \ll \varepsilon_e$ ,  $\bar{\varepsilon}$  degenerates to the effective strain  $\varepsilon_e$ , and Eq. (10) degenerates to the strain energy density in classical plasticity.

### 3. Pure bending specimen

The pure bending specimen is studied in this section. The solution also serves as the basis for the analysis of other microbend test specimens in Sections 4 and 5. Let  $x_1$  be the neutral axis of the beam, and the bending is within the  $x_1$ – $x_2$  plane. The in-plane strains and curvatures are  $\varepsilon_{11}$ ,  $\varepsilon_{22}$ ,  $\varepsilon_{12}$ ,  $\chi_1$  and  $\chi_2$ . The strain  $\varepsilon_{11}$  along the axial direction and the shear strain  $\varepsilon_{12}$  in pure bending are given by

$$\varepsilon_{11} = \kappa x_2, \quad \varepsilon_{12} = 0, \quad (12)$$

where  $\kappa$  is the constant curvature of the beam in pure bending. The out-of-plane width (in the  $x_3$  direction) is usually much larger than the thickness (in the  $x_2$  direction) of microbend test specimens (Stolken and Evans, 1998; Haque and Saif, in press) such that the beam is subjected to plane-strain deformation,  $\varepsilon_{33} = 0$ . The incompressibility of plastic deformation and the plane-strain condition  $\varepsilon_{33} = 0$  give  $\varepsilon_{22} = -\varepsilon_{11} = -\kappa x_2$ . The curvatures in pure bending are obtained from the  $\chi$ – $\varepsilon$  compatibility (5) as

$$\chi_1 = -\kappa, \quad \chi_2 = 0. \quad (13)$$

For an incompressible solid, the constitutive law (7) only gives the deviatoric stresses and couple stresses. The hydrostatic stress has to be determined from equilibrium equations and vanishing of normal stress traction on the top and bottom surfaces of the beam. The non-vanishing stress and couple stress in pure bending are given by

$$\sigma_{11} = \frac{4}{3} \frac{\sigma_0}{\varepsilon_0^{1/n}} |\kappa|^{1/n} \kappa \left( \frac{4}{3} x_2^2 + \frac{2}{3} l^2 \right)^{\frac{1-n}{2n}} x_2, \quad (14)$$

and

$$m_1 = -\frac{2}{3} l^2 \frac{\sigma_0}{\varepsilon_0^{1/n}} |\kappa|^{1/n} \kappa \left( \frac{4}{3} x_2^2 + \frac{2}{3} l^2 \right)^{\frac{1-n}{2n}}. \quad (15)$$

It can be verified that the stress and couple stress in Eqs. (14) and (15) satisfy equilibrium Eqs. (1) and (2), boundary conditions (3), and the corresponding strain and curvature fields in Eqs. (12) and (13) satisfy the compatibility Eqs. (5) and (6). Therefore, this is an exact solution.

The bending moment  $M$  (per unit width of the beam) can be determined from the normal stress  $\sigma_{11}$  and couple stress  $m_1$ ,

$$\int_{-\frac{h}{2}}^{\frac{h}{2}} \sigma_{11} x_2 dx_2 - \int_{-\frac{h}{2}}^{\frac{h}{2}} m_1 dx_2 = M, \tag{16}$$

which yields a power-law relation between the curvature  $\kappa$  and the bending moment  $M$ ,

$$M = \frac{\sigma_0}{\varepsilon_0^{1/n}} I |\kappa|^{\frac{1-n}{n}} \kappa, \tag{17}$$

where  $I$  is the *modified moment of inertia* to account for the strain gradient effects, given by

$$I = \int_{-\frac{h}{2}}^{\frac{h}{2}} \left( \frac{4}{3} x_2^2 + \frac{2}{3} l^2 \right)^{\frac{n+1}{2n}} dx_2. \tag{18}$$

It is observed from Eqs. (17) and (18) that the strain gradient effects come into play only by increasing the modified moment of inertia  $I$ . In the limit of  $h \gg l$  (beam thickness  $\gg$  the intrinsic material length), the modified moment of inertia degenerates to that for classical plasticity,

$$I_0 = I(l = 0) = \frac{n}{\sqrt{3}(2n + 1)} \left( \frac{h}{\sqrt{3}} \right)^{1/n} h^2. \tag{19}$$

The elastic couple stress theory (Toupin, 1962; Koiter, 1964; Mindlin, 1964, 1965) corresponds to the limit  $n = 1$  at which Eqs. (17) and (18) still hold except that the bending stiffness  $\sigma_0 \varepsilon_0^{-1/n} I$  is replaced by  $\frac{1}{12} \frac{E}{1-\nu^2} h^3 + 2G l^2 h$ , where  $E$ ,  $G$  and  $\nu$  are Young’s modulus, shear modulus, and Poisson’s ratio, respectively. It is evident that the first term  $\frac{1}{12} \frac{E}{1-\nu^2} h^3$  represents the conventional elastic bending stiffness (in plane strain), while the second term  $2G l^2 h$  is the contribution from strain gradient effects. For a rigid-perfectly plastic solid ( $n = \infty$ ) with strain gradient effects, the modified moment of inertia  $I$  is given explicitly by

$$I = \frac{h^2}{2\sqrt{3}} \sqrt{1 + \frac{2l^2}{h^2}} + \frac{l^2}{\sqrt{3}} \ln \left( \frac{h}{\sqrt{2}l} + \sqrt{1 + \frac{h^2}{2l^2}} \right). \tag{20}$$

The modified moment of inertia  $I$  normalized by its counterpart  $I_0$  in classical plasticity is presented versus the ratio of intrinsic material length to beam thickness,  $l/h$ , in Fig. 2 for the plastic work hardening exponent  $n = 5, 10$  and  $\infty$ . The limit  $n = \infty$  corresponds to a rigid-perfectly plastic solid, while the limit  $l/h = 0$  corresponds to classical plasticity. The ratio  $I/I_0$  for the elastic couple stress theory ( $n = 1$ ) is also presented in Fig. 2 (the Poisson’s ratio  $\nu = 0.3$ ). It is observed that the modified

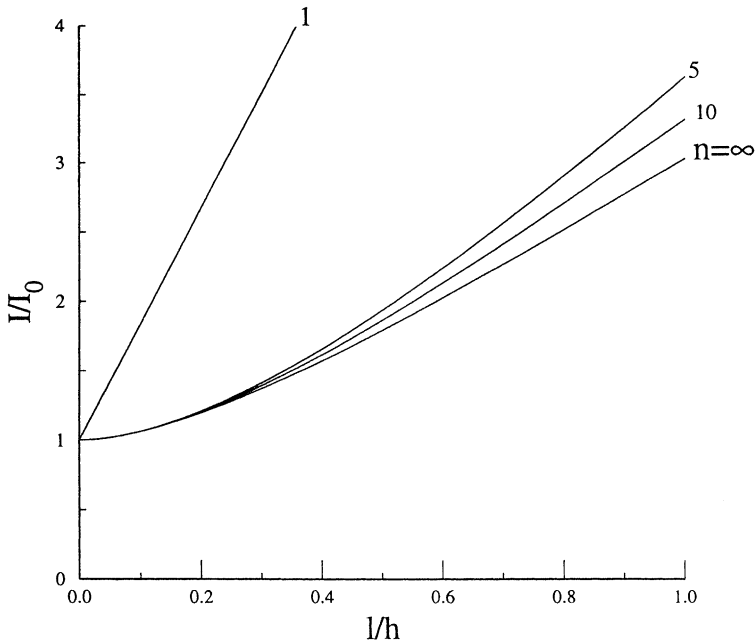


Fig. 2. The modified moment of inertia in strain gradient plasticity normalized by its counterpart in conventional plasticity,  $I/I_0$ , versus the ratio of intrinsic material length to beam thickness,  $l/h$ , for the plastic work hardening exponent  $n=5, 10$  and  $\infty$ , where  $n=\infty$  corresponds to a perfectly plastic solid. The ratio  $I/I_0$  for  $n=1$  is also presented with the Poissons ratio  $\nu=0.3$ .

moment of inertia  $I$  increases rapidly when the beam thickness  $h$  becomes comparable to the intrinsic material length  $l$ . For  $h=l$  and  $n=10$ ,  $I$  is more than three times larger than  $I_0$ . Therefore, the strain gradient effects significantly increase the effective bending stiffness of a microbend test specimen when the beam thickness is on the order of microns. It is also observed that the curves for  $n=5$  and  $n=\infty$  in Fig. 2 are rather close, indicating the dependence of the modified moment of inertia  $I$  on the plastic work hardening exponent  $n$  is rather weak so that the analytical expression in Eq. (20) is a good approximation for the typical range of plastic work hardening exponent,  $5 \leq n \leq \infty$ .

Fig. 2 is important to the design of a microbend test specimen in order to determine the intrinsic material length  $l$  in strain gradient plasticity. Strain gradient effects appear only through the modified moment of inertia  $I$  in Eq. (18). For strain gradient effects to be important in bending, the beam must be thin enough such that the modified bending moment of inertia  $I$  is significantly larger than its counterpart  $I_0$  in classical plasticity. For  $I$  to be twice  $I_0$ , the beam thickness  $h$  needs to be approximately twice the intrinsic material length  $l$ , which suggests that the beam thickness should be on the order of 10 microns in order to fully capture the strain gradient effects. This is indeed on the same order as that used by Stolken and Evans (1998).

The power-law relation (17) between the normalized bending moment,  $M/(\sigma_0 \varepsilon_0^{-1/n} h^2)$ , and the normalized curvature,  $\kappa h$ , is shown in Fig. 3 for the plastic

work hardening exponent  $n=5$  and various ratios of intrinsic material length to beam thickness,  $l/h$ . The curve for  $l/h=0$  corresponds to classical plasticity. This  $M-\kappa$  relation depends strongly on the beam thickness  $h$  when it is on the order of microns. For example, in Stolken and Evans' (1998) microbend test of nickel beam, the beam thickness ( $12.5 \mu\text{m}$ ) was slightly more than twice the intrinsic material length ( $5 \mu\text{m}$ ). For a displacement-controlled bending experiment (given  $\kappa$ ), the bending moment corresponding to  $l/h=1/2$  in Fig. 3 for strain gradient plasticity is almost twice that for classical plasticity ( $l/h=0$ ). With the same beam thickness  $h=2l$ , the curvature for strain gradient plasticity in a load-controlled bending experiment (given  $M$ ) is only 4.5% of that for classical plasticity, indicating the deformation is significantly reduced due to strain gradient effects. However, when the beam thickness becomes ten times the intrinsic material length ( $h=10l$ ), the corresponding curve in Fig. 3 is very close to that for classical plasticity ( $l/h=0$ ), and the strain gradient effects become insignificant.

For a beam undergoing finite rotation, as observed in aforementioned experiments (Stolken and Evans, 1998; Haque and Saif, in press), the curvature is related to the slope  $\theta$  of the deformed beam by

$$\kappa = -\frac{d\theta}{ds}, \tag{21}$$

where  $s$  is the arc length along the neutral axis of the deformed beam. The constant curvature in pure bending indicates that the beam is bent to a circle with radius

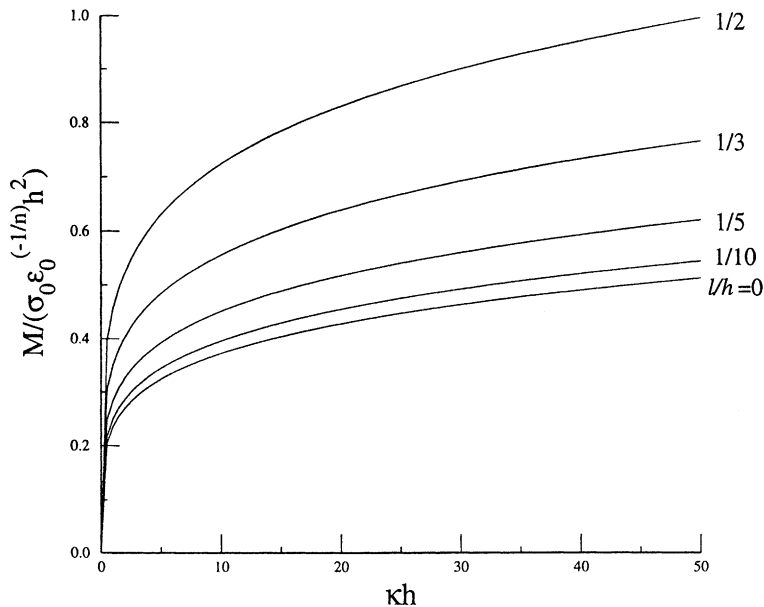


Fig. 3. The normalized bending moment,  $M/(\sigma_0 \epsilon_0^{-1/n} h^2)$ , versus the normalized curvature,  $\kappa h$ , for the plastic work hardening exponent  $n=5$  and various ratios of intrinsic material length to beam thickness,  $l/h$ , in pure bending. The curve for  $l/h=0$  corresponds to classical plasticity.

$1/|\kappa|$ . The lateral deflection (normal to the beam axis  $x_1$  in the undeformed configuration) for a clamped beam subjected to pure bending  $M$  can be found as

$$v = -\left(\frac{|M|}{\sigma_0 \varepsilon_0^{-1/n} I}\right)^{-n} \left\{ 1 - \cos \left[ \left(\frac{|M|}{\sigma_0 \varepsilon_0^{-1/n} I}\right)^n s \right] \right\} \text{sign}(M), \quad 0 \leq s \leq L. \quad (22)$$

The deformed beam is shown in Fig. 4 for various ratios of intrinsic material length to beam thickness,  $l/h$ . The plastic work hardening exponent is  $n=5$ , and the bending moment is chosen at a relatively large value,  $M = \frac{n\sigma_0 h^2}{\sqrt{3(2n+1)}} \left(\frac{h}{\sqrt{3}\varepsilon_0 L}\right)^{1/n}$ , in order to display the effect of finite rotation. The curve for  $l/h=0$  corresponds to classical plasticity. As the beam thickness  $h$  decreases to twice the intrinsic material length (Stolken and Evans, 1998), the lateral deflection at the end of the cantilever beam in Fig. 4 for strain gradient plasticity is only 3.9% of that for classical plasticity.

#### 4. Cantilever beam

Haque and Saif (in press) developed a microbend cantilever beam subjected to a concentrated load at the end. This specimen is analyzed in this section. For a cantilever

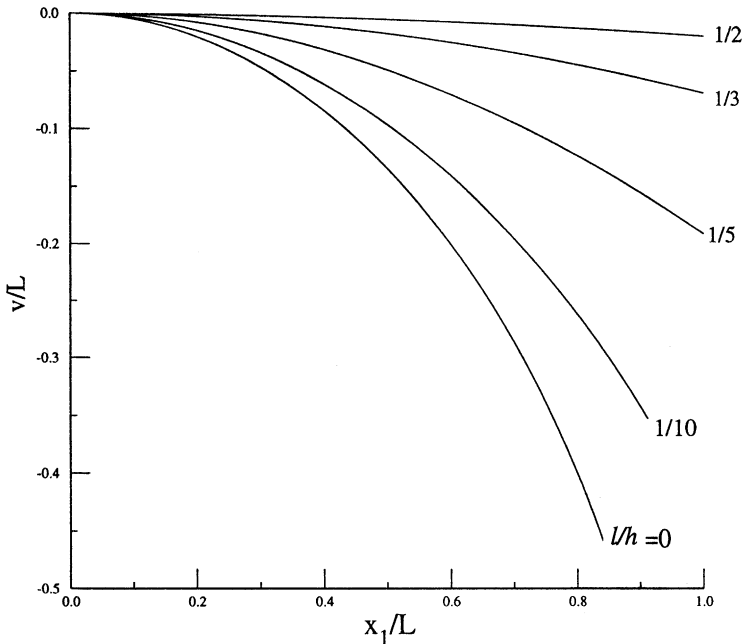


Fig. 4. The deformed beam in pure bending for various ratios of intrinsic material length to beam thickness,  $l/h$ ; the plastic work hardening exponent  $n=5$ , and the bending moment  $M = \frac{n\sigma_0 h^2}{\sqrt{3(2n+1)}} \left(\frac{h}{\sqrt{3}\varepsilon_0 L}\right)^{1/n}$ . The curve for  $l/h=0$  corresponds to classical plasticity.

beam undergoing finite rotation, the concentrated load at the end is not normal to the deformed beam axis such that the beam is subjected to combined bending and stretching. The elongation associated with this axial stretching force is much smaller than the deformation due to bending and can therefore be neglected. However, this axial stretching force is important in the equilibrium of the beam. A beam element with the bending moment  $M$ , shear force  $V$  and axial force  $N$  is shown in Fig. 5. Force and moment equilibrium give

$$\frac{dM}{ds} = V, \quad \frac{dV}{ds} + N \frac{d\theta}{ds} = 0, \quad \frac{dN}{ds} - V \frac{d\theta}{ds} = 0, \quad (23)$$

where  $\theta$  is the slope of the deformed beam, and is related to the curvature and moment via Eqs. (17) and (21) by

$$\frac{d\theta}{ds} = -\left(|M|\varepsilon_0^{1/n}/\sigma_0 I\right)^n \text{sign}(M). \quad (24)$$

Eqs. (23) and (24) constitute the governing equations for  $M$ ,  $V$ ,  $N$  and  $\theta$ . The corresponding boundary conditions are obtained from the moment at the free end, the shear and axial forces and the slope at the clamped end, i.e.

$$\begin{aligned} M(s=L) &= 0, & V(s=0) &= -P, \\ N(s=0) &= 0, & \theta(s=0) &= 0, \end{aligned} \quad (25)$$

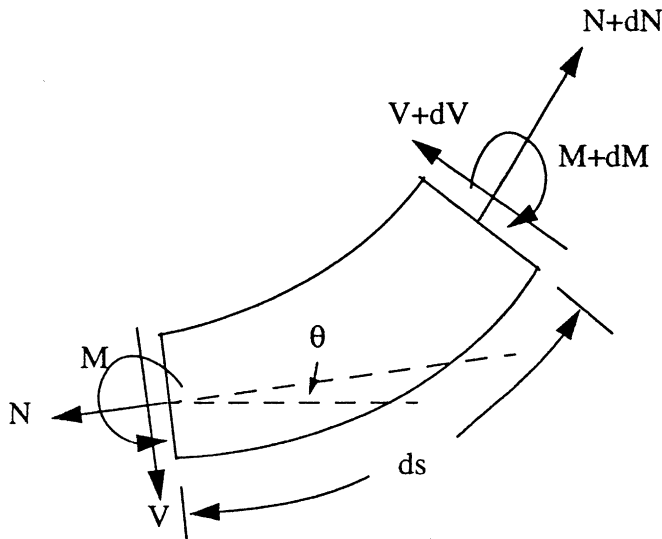


Fig. 5. A schematic diagram of a beam element subjected to the bending moment  $M$ , shear force  $V$  and axial force  $N$ . The slope of the beam's neutral axis is  $\theta$ .

where  $L$  is the initial length of the beam. Eqs. (23) and (24) with the boundary conditions (25) must be solved numerically. Once the slope  $\theta$  is obtained, the lateral deflection  $v$  of the beam is found as

$$v = \int_0^s \sin\theta ds. \tag{26}$$

The deformed beam is presented in Fig. 6 for various ratios of intrinsic material length to beam thickness,  $l/h$ . The plastic work hardening exponent is  $n=5$ , and the load is chosen at  $P = \frac{n\sigma_0 h^2}{\sqrt{3}(2n+1)L} \left(\frac{h}{\sqrt{3}\epsilon_0 L}\right)^{1/n}$  such that the maximum moment at the clamped end is the same as the moment as in Fig. 4 for pure bending. As the beam thickness  $h$  decreases to twice the intrinsic material length (Stolken and Evans, 1998), the lateral deflection at the end of the cantilever beam in Fig. 6 for strain gradient plasticity is only 3.8% of that for classical plasticity, which is very close to the corresponding estimate of 3.9% for the pure bending specimen (Fig. 4).

**5. The microbend test**

Stolken and Evans (1998) developed a microbend test in order to determine the intrinsic material length  $l$  of nickel. A schematic diagram of the experimental setup is

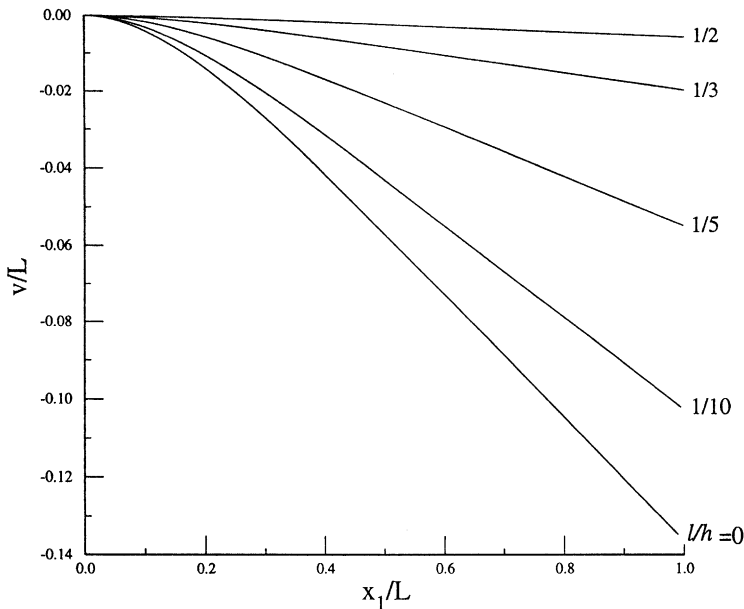


Fig. 6. The deformed cantilever beam for various ratios of intrinsic material length to beam thickness,  $l/h$ ; the plastic work hardening exponent  $n=5$ , and the load  $P = \frac{n\sigma_0 h^2}{\sqrt{3}(2n+1)L} \left(\frac{h}{\sqrt{3}\epsilon_0 L}\right)^{1/n}$ . The curve for  $l/h=0$  corresponds to classical plasticity.

shown in Fig. 7a. A nickel beam is clamped between two tungsten wires and the beam is bent by the bend dies applied at both ends of the beam. The thickness of the beam is  $h = 12.5, 25$  and  $50 \mu\text{m}$ ; the initial half length of the beam is  $L = 3 \text{ mm}$ . The diameter of the tungsten wires is  $D = 0.125, 0.25, 0.5, 1$  and  $2 \text{ mm}$ . The beam undergoes large plastic deformation, and then complete unloading. The deformation of tungsten wires is much smaller than the nickel beam such that the tungsten wires are modeled as rigid wires. As the deformation reaches a critical state, the contact between the nickel beam and the tungsten wire changes from the point contact to a finite contact zone, and the contact zone size increases with the loading. In the present study, the

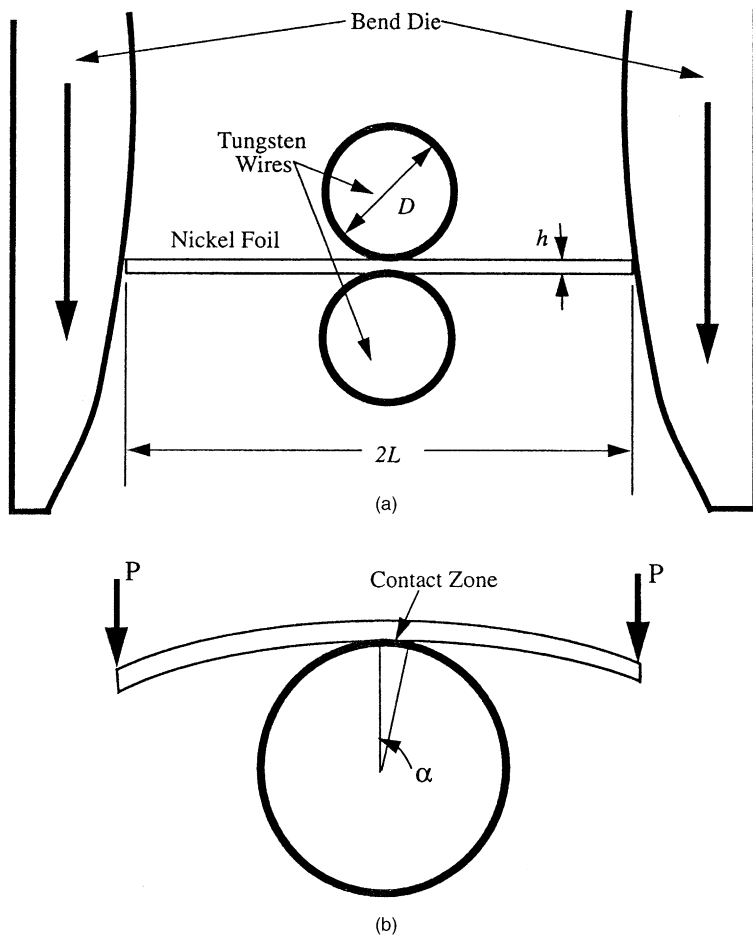


Fig. 7. A schematic diagram of the microbend test. (a) Experimental setup: an ultra-thin nickel beam clamped between two tungsten wires and bent by the bend dies applied at both ends of the beam. (b) Modeling: an ultra-thin beam on top of a rigid wire subjected to a lateral load  $P$  at the end. The contact angle is denoted by  $\alpha$ .

microbend test is modeled as a cantilever beam on top of a rigid wire and the beam is subjected to a lateral load  $P$  at the end (Fig. 7b).

The governing Eqs. (23) and (24) still apply outside the contact zone, i.e.  $\frac{D}{2}\alpha \leq s \leq L$ , where  $D$  is the diameter of the tungsten wire,  $\alpha$  is the contact angle, and  $L$  is the half of the initial length of the beam. The corresponding boundary conditions are imposed at the end of the beam ( $s=L$ ) and at the end of contact zone ( $s=D\alpha/2$ ). The moment at the beam end  $s=L$  and the shear and axial forces at the end of the contact zone  $s=\frac{D}{2}\alpha$  are

$$M(s=L)=0, \quad V\left(s=\frac{D}{2}\alpha\right)=-P\cos\alpha, \quad N\left(s=\frac{D}{2}\alpha\right)=P\sin\alpha. \quad (27)$$

The slope and curvature of the beam are the same as those of the rigid wire at the end of contact zone, i.e.

$$\theta\left(s=\frac{D}{2}\alpha\right)=-\alpha, \quad \kappa\left(s=\frac{D}{2}\alpha\right)=\frac{2}{D}. \quad (28)$$

The second boundary condition in the above equation can be equivalently written for the moment at the end of contact zone via the  $M$ - $\kappa$  relation (17) as

$$M\left(s=\frac{D}{2}\alpha\right)=\frac{\sigma_0}{\varepsilon_0^{1/n}}I\left(\frac{2}{D}\right)^{1/n}. \quad (29)$$

Eqs. (23) and (24) with the boundary conditions (27) and the first boundary condition in (28) are solved numerically for each given contact angle  $\alpha$ . The as-yet-unknown contact angle  $\alpha$  is determined by the extra boundary condition in Eq. (29). Therefore, for a given load  $P$ , an iteration process is necessary to determine the contact angle  $\alpha$ . Once the slope  $\theta$  is obtained, the lateral deflection  $v$  of the beam is given by

$$v=-\frac{D}{2}(1-\cos\alpha)+\int_{\frac{D}{2}\alpha}^s \sin\theta ds. \quad (30)$$

The deformed beam is presented in Fig. 8 for various levels of load  $P$ . The material properties are Young's modulus  $E=207$  GPa, Poisson's ratio  $\nu=0.312$ , uniaxial stress-strain relation  $\sigma=610 \varepsilon^{0.56}$  MPa, and intrinsic material length  $l=5$   $\mu$ m. The microbend test specimen has the beam thickness  $h=12.5$   $\mu$ m, beam length  $L=3$  mm, and wire diameter  $D=0.5$  mm. The straight line for  $P=0$  corresponds to the initial, undeformed configuration. The effect of finite rotation of the beam is clearly observed when the load  $P$  (per unit width of the beam) is 0.54 N/m (Newton per meter). Before the load reaches 9.13 N/m, the beam and the rigid wire retain point contact, though the beam has been bent severely. As the load  $P$  exceeds 9.13 N/m, a finite contact zone is developed between the beam and the wire, and the contact zone

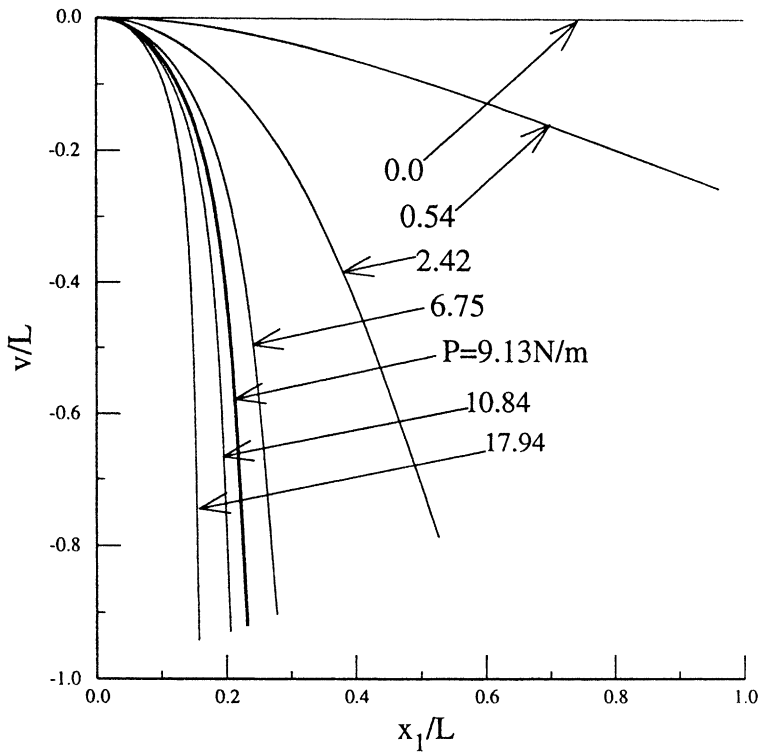


Fig. 8. The microbend test of a nickel beam under various levels of loading  $P$ ; the nickel beam has the Young's modulus  $E=207$  GPa, Poisson's ratio  $\nu=0.312$ , uniaxial stress–strain relation  $\sigma=610e^{0.56}$  MPa, intrinsic material length  $l=6$   $\mu\text{m}$ , the beam thickness  $h=12.5$   $\mu\text{m}$ , beam length  $L=3$  mm, and the diameter of tungsten wires  $D=0.5$  mm.

size increases with the load. When the load  $P$  reaches 10.84 and 17.94 N/m, the contact lengths are 0.044 and 0.131 mm, respectively, and the corresponding contact angles are  $\alpha=10^\circ$  and  $\alpha=30^\circ$ .

## 6. Discussion

We have analyzed three microbend test specimens with the phenomenological theory of strain gradient plasticity, namely the pure bending specimen, cantilever beam in Haque and Saif's (in press) experiments, and the microbend test specimen developed by Stolken and Evans (1998). The effect of finite rotation of the beam has been considered since these microbend tests undergo large deflections (Stolken and Evans, 1998; Haque and Saif, in press). Strain gradient effects are significant when the beam thickness becomes comparable to the intrinsic material length  $l$  ( $\sim 4$   $\mu\text{m}$  for copper and 5  $\mu\text{m}$  for nickel) of strain gradient plasticity. When the beam thickness  $h$  equals  $l$ , the bending stiffness in strain gradient plasticity exceeds three times

that in classical plasticity such that the deflection estimated by strain gradient plasticity is only a few percent of that in classical plasticity. However, as the beam thickness increases to 10 times the intrinsic materials, strain gradient effects become rather small.

The analysis in the present paper serves two purposes. First, such an analysis is generally necessary for the estimation of the intrinsic material length  $l$  in strain gradient plasticity from the microbend tests (e.g. Haque and Saif, in press). Second, the analysis can help in determining which microbend tests are the most suitable for the experimental measurement of intrinsic material length  $l$ . For example, we have examined a double cantilever beam (both ends clamped) subjected to a normal concentrated load  $P$  at the center. It is found that the difference in lateral deflection between classical plasticity ( $l/h=0$ ) and strain gradient plasticity ( $l/h=1/2$ ) is rather small. Even for a very large load  $P= Eh$  ( $E$  – Young's modulus,  $h$  – beam thickness), the difference in the lateral deflection at the center is less than 25%, which is much smaller than that for the pure bending specimen, cantilever beam, and microbend specimen in Sections 3–5. This is because the axial force  $N$  is very large in the double cantilever beam such that the uniform axial stretch overwhelms the strain gradient effects in bending. For example, for  $P= Eh$ , the axial force  $N$  at the clamped ends is more than 8 times  $P$  for  $l/h=1/2$ , while the corresponding bending moment at the clamped ends is only  $0.014PL$  ( $L$  – beam length). Therefore, the double cantilever beam is an unsuitable specimen for measuring the intrinsic material length parameter in strain gradient plasticity.

## Acknowledgements

Y.H. gratefully acknowledges the helpful discussion with J.S. Stolken of the University of California at Santa Barbara, C. Liu of Los Alamos National Laboratory, and the support from NSF (No. CMS-00-84980) and from Motorola Foundation. K.J.H. gratefully acknowledges the support from NSF (Grant No. CMS-95-22661).

## References

- Acharya, A., Bassani, J.L., 2000. Lattice incompatibility and a gradient theory of crystal plasticity. *J. Mech. Phys. Solids* 48, 1565–1595.
- Aifantis, E.C., 1987. The physics of plastic deformation. *Int. J. Plasticity* 3, 211–247.
- Aifantis, E.C., 1999. Strain gradient interpretation of size effects. *Int. J. Fracture* 95, 299–314.
- Ashby, M.F., 1970. The deformation of plastically non-homogeneous alloys. *Philos. Mag.* 21, 399–424.
- Chau, K., Allegretto, W., Ristic, L.J., 1991. Simulation of silicon microstructures. *Sensors and Materials* 2, 253–280.
- Cottrell, A.H., 1964. *The Mechanical Properties of Materials*, John Wiley & Sons, p. 277.
- Dai, H., Parks, D.M., 2001. Geometrically-Necessary Dislocation Density in Continuum Crystal Plasticity Theory and FEM Implementation (unpublished work).
- Dillon, O.W., Kratochvil, J., 1970. A strain gradient theory of plasticity. *Int. J. Solids Structures* 6, 1513–1533.

- Engelen, R.A.B., Geers, M.G.D., Baaijens, F.P.T., in press. Nonlocal implicit gradient-enhanced elasto-plasticity for the modeling of softening behavior. *Int. J. Plasticity*.
- Fleck, N.A. and Hutchinson, J.W., 1993. A phenomenological theory for strain gradient effects in plasticity. *J. Mech. Phys. Solids* 41, 1825–1857.
- Fleck, N.A., Hutchinson, J.W., 1997. Strain gradient plasticity. *Advances in Applied Mechanics* 33, 295–361.
- Fleck, N.A., Muller, G.M., Ashby, M.F., Hutchinson, J.W., 1994. Strain gradient plasticity: theory and experiment. *Acta Metall. Mater.* 42, 475–487.
- Gao, H., Huang, Y., Nix, W.D., Hutchinson, J.W., 1999. Mechanism-based strain gradient plasticity, I—theory. *J. Mech. Phys. Solids* 47, 1239–1263.
- Geijselers, H.J.M., Tjeldeman, H., 1991. The dynamic mechanical characteristics of a resonating micro-bridge mass-flow sensor. *Sensors and Actuators* 29, 37–41.
- Gurtin, M.E., in press. On a framework for small-deformation viscoplasticity: free energy, microforces, strain gradients. *Int. J. Plasticity*.
- Haque, A., Saif, M.T.A., in press. Bending experiment on a 100nm thin Al cantilever beam using MEMS: effect of strain gradient.
- Huang, Y., Gao, H., Nix, W.D., Hutchinson, J.W., 2000a. Mechanism-based strain gradient plasticity, II—Analysis. *J. Mech. Phys. Solids* 48, 99–128.
- Huang, Y., Xue, Z., Gao, H., Nix, W.D., Xia, Z.C., 2000b. A study of micro-indentation hardness test by mechanism-based strain gradient plasticity. *J. Mater. Res.* 15, 1786–1796.
- Hwang, K.C., Jiang, H., Huang, Y., Gao, H., in press. Finite deformation analysis of mechanism-based strain gradient plasticity: torsion and crack tip field. *Int. J. Plasticity*.
- Koiter, W.T., 1964. Couple stresses in the theory of elasticity, I and II. *Proc. Ned. Akad. Wet. (B)* 67, 17–44.
- Lloyd, D.J., 1994. Particle reinforced aluminum and magnesium matrix composites. *Int. Mater. Rev.* 39, 1–23.
- Ma, Q., Clarke, D.R., 1996. Size dependent hardness of silver single crystals. *J. Mater. Res.* 10, 853–863.
- McElhaney, K.W., Vlassak, J.J., Nix, W.D., 1998. Determination of indenter tip geometry and indentation contact area for depth-sensing indentation experiments. *J. Mater. Res.* 13, 1300–1306.
- Mindlin, R.D., 1964. Micro-structure in linear elasticity. *Archive Rational Mechanics Analysis* 16, 51–78.
- Mindlin, R.D., 1965. Second gradient of strain and surface tension in linear elasticity. *Int. J. Solids Struct.* 1, 417–438.
- Nan, C.-W., Clarke, D.R., 1996. The influence of particle size and particle fracture on the elastic/plastic deformation of metal matrix composites. *Acta Mater.* 44, 3801–3811.
- Nix, W.D., 1988. Mechanical properties of thin films. *Metall. Trans. A* 20A, 2217–2245.
- Nix, W.D., Gao, H., 1998. Indentation size effects in crystalline materials: A law for strain gradient plasticity. *J. Mech. Phys. Solids* 46, 411–425.
- Nix, W.D. and Gibeling, J.C., 1985. Mechanism of time-dependent flow and fracture of metals. In: *Metals/Materials Technology Series 8313-004*, ASM, Metals Park, OH.
- Nye, J.F., 1953. Some geometrical relations in dislocated crystals. *Acta Metall.* 1, 153–162.
- Poole, W.J., Ashby, M.F., Fleck, N.A., 1996. Micro-hardness of annealed and work-hardened copper polycrystals. *Scripta Metall. Mater.* 34, 559–564.
- Rhee, M., Hirth, J.P., Zbib, H.M., 1994a. A superdislocation model for the strengthening of metal matrix composites and the initiation and propagation of shear bands. *Acta Metall. Mater.* 42, 2645–2655.
- Rhee, M., Hirth, J.P., Zbib, H.M., 1994b. On the bowed out tilt wall model of flow stress and size effects in metal matrix composites. *Scripta Metall. Mater.* 31, 1321–1324.
- Saif, M.T.A., MacDonald, N.C., 1998. Measurement of forces and spring constants of microinstruments. *Rev. Scientific Instrum.* 69, 1410–1422.
- Shu, J.Y., Barlow, C.Y., 2000. Strain gradient effects on microscopic strain field in a metal matrix composite. *Int. J. Plasticity* 16, 563–591.
- Stelmashenko, N.A., Walls, A.G., Brown, L.M., Milman, Y.V., 1993. Microindentations on W and Mo oriented single crystals: an STM study. *Acta Metall. Mater.* 41, 2855–2865.

- Stolken, J.S., Evans, A.G., 1998. A microbend test method for measuring the plasticity length scale. *Acta Mater.* 46, 5109–5115.
- Toupin, R.A., 1962. Elastic materials with couple stresses. *Archive Rational Mechanics Analysis* 11, 385–414.
- Zhu, H.T., Zbib, H.M., 1995. Flow strength and size effect of an Al–Si–Mg composite model system under multiaxial loading. *Scripta Metall. Mater.* 32, 1895–1902.
- Zhu, H.T., Zbib, H.M., Aifantis, E.C., 1997. Strain gradients and continuum modeling of size effect in metal matrix composites. *Acta Mechan.* 121, 165–176.